Quasi Resonant LED Driver with Coupled Current Doubler Rectifier

Alexander Abramovitz, Alexander Bazarov and Doron Shmilovitz
Tel-Aviv University
Ramat Aviv, 6978
Tel-Aviv, Israel
Tel.: 972 - 03-6406238
E-Mail: alabr@hotmail.com, shmilo@post.tau.ac.il
URL: http://www.eng.tau.ac.il/~shmilo/

Keywords

«Electronic ballast», «Lighting», «ZCZVS converters»

Abstract

This paper describes the topology and operation of a quasi-resonant driver for LED lighting applications. The proposed driver incorporates a current doubler rectifier and capacitive safety isolation barrier. Variable frequency constant on-time dimming strategy is employed. Capacitive isolation helps eliminating the isolation transformer. The proposed theory is suggested and verified by simulation and experiment.

Introduction

High brightness LEDs (HB LED) are a promising solution to lighting applications [1]-[2]. An off-line HB LED requires a miniature AC-DC power converter, referred to as LED driver, also has to be reliable and affordable. Therefore, LED drivers are in the focus of recent research activities [3]-[6].
An additional feature of the proposed topology is the capacitive isolation from AC mains which allows operation with no transformer. This poses a relatively high operation frequency that requires operation in quasi-resonant mode. Having a diode-like *i-v* characteristic, LED is, in a way, a special type of load requiring a particular matching. Source-load characteristic matching was attended in [7] - [9]. LEDs prefer constant current operation. LED drivers with current control can also provide a precise dimming function. Therefore, LED drivers should, in a way, exhibit gyrator characteristics [10] - [13].

I. The Proposed Topology

The proposed here topology of the Quasi Resonant LED Driver with Coupled Current Doubler Rectifier (CCD-QRLEDD) is shown in Fig. 1 (a). The proposed circuit was derived from an earlier version [6] by modifying the output rectifier stage with a coupled current doubler rectifier. Compared to the earlier counterpart CCD-QRLEDD provides reduced crest factor and can be operated at higher frequency. An additional merit of CCD-QRLEDD is a single ground referenced switch. Furthermore, CCD-QRLEDD operates in a quasi-resonant mode with discontinuous input and the output currents. Furthermore, CCD-QRLEDD has inherent resistive input characteristics and thus attains low distortion and high power factor. Moreover, CCD-QRLEDD also provides inherent zero current turn-on and zero voltage switching turn-off conditions to the power switch so the switching loss is minimized.
The simplified model of the CCD-QRLEDD shown in Fig. 1 (b) is constructed based on the following assumptions:

a) the CCD-QRLEDD operates in the quasi-steady state equilibrium in the vicinity of a certain value of the input voltage, V_i;
b) the operating voltage of the LED string, V_{LED}, is constant;
c) the equivalent capacitor, C_s, represents the pair of series blocking capacitors;
d) ideal semiconductor switches.

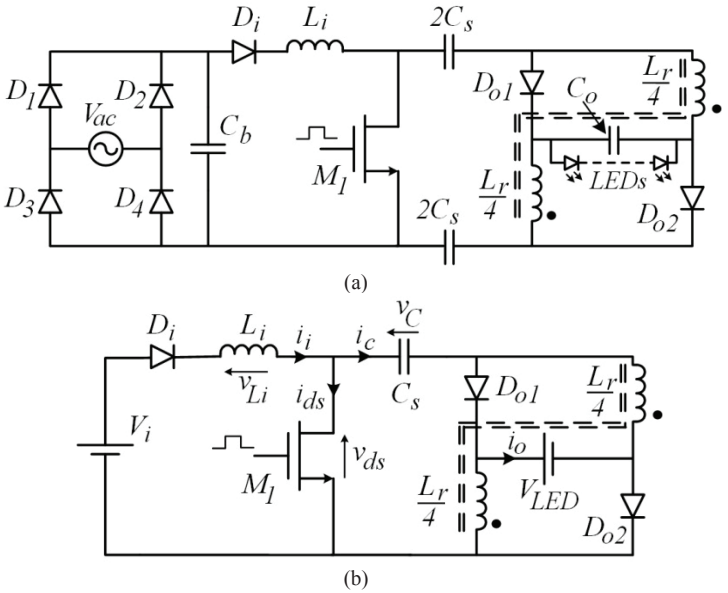

Fig. 1. Proposed CCD-QRLEDD topology (a); and its simplified equivalent circuit (b).

II. Analysis of Operation

Typical waveforms of the proposed CCD-QRLEDD on the line frequency and on the switching frequency scale are illustrated in Fig. 2. The simulated average line current waveform, i_{ac_av}, shown in Fig. 2 (a) on the line period scale, appears as a near sinusoidal signal, which manifests that the CCD-QRLEDD possesses inherent resistive input characteristic, high power factor and low harmonic content. Examining the switch waveforms, shown in Fig. 2 (b) on the switching period scale, reveals favorable zero current (ZC) turn on and zero voltage (ZV) turn off switching of the MOSFET switch, which are a prerequisite to attain high efficiency at high frequency.

Analysis of the CCD-QRLEDD waveforms in Fig. 2 (b) reveals that the switching cycle of CCD-QRLEDD has five topological states. The equivalent circuits are show in Fig. 3.

State A: t_0-t_1, see Fig. 3 (a), commences when M_1 is turned on. The switching occurs at zero current condition. Here, L_i begins charging from the input source, V_i, via D_i, while C_s and L_r are allowed to resonate. Here, L_r represents the magnetizing inductance of both series connected windings of the coupled inductor.

State B: t_1-t_2, see Fig. 3 (b), commences as D_{o1} and D_{o2} begin conducting. Hence, the coupled inductor windings are reconfigured so that both windings can discharge towards the output, V_{LED}, in parallel. The equivalent inductance of each winding is $L_r/4$. Meanwhile C_s is clamped to the negative of the output voltage (- V_{LED}) and since M_1 is still on, the inductor L_i keeps charging.

State C: t_2-t_3, see Fig. 3 (c), commences when the switch, M_1, is turned off, which occurs at zero voltage, v_{ds}=0, thanks to C_s snubbing. As L_i and C_s resonate the capacitor C_s is charged to high voltage while the diodes D_{o1} and D_{o2}, conduct the resonant current to the output. In the interim the coupled inductor keeps discharging to the output, V_{LED}. State C ends as the inductor L_i is discharged and the diode, D_i, turns off at zero current.

State D: t_3-t_4, see Fig. 3 (d), commences upon the turn off of the diode D_i. Both coupled inductor windings, $L_r/4$ continue to discharge the stored energy to the output while the capacitor, C_s, preserves its state. When the coupled inductor, L_r, is totally discharged, the diodes, D_{o1} and D_{o2}, turn off at zero current terminating State D.

State E: t_4- t_5, see Fig. 3 (e), is the idle state. Here, inductors carry no current and the capacitor, C_s, preserves its state.

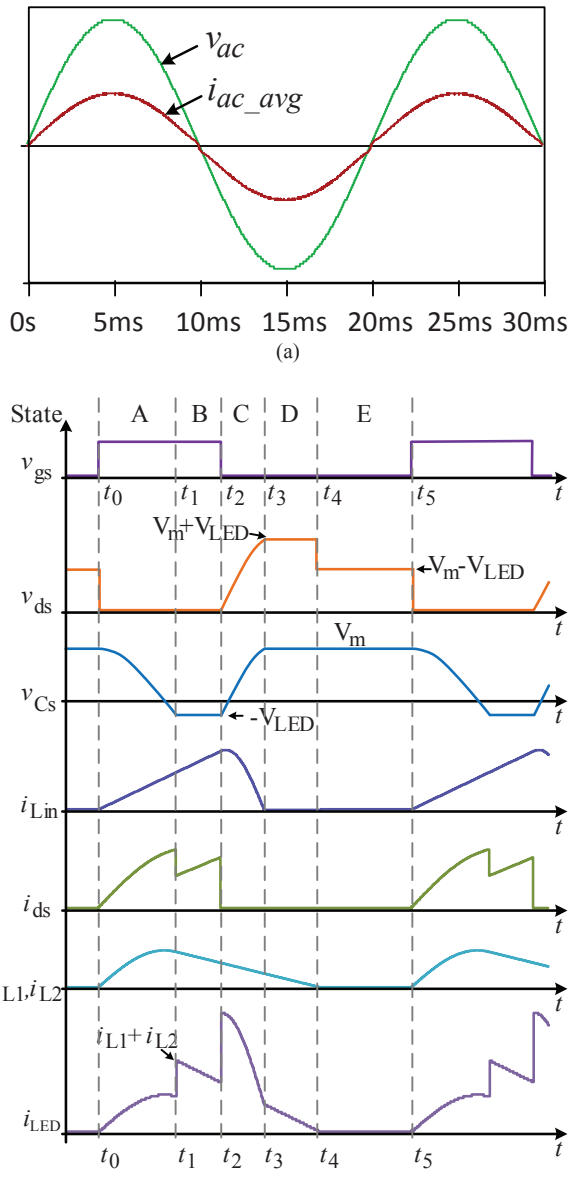

Fig. 2. Key waveforms of the proposed CCD-QRLEDD (a) on the line cycle scale: outer-line voltage, Vac, inner- average line current, iac_avg. (b) key waveforms on the switching period scale.

The proposed CCD-QRLEDD is conceived to be controlled by variable frequency constant on time switching signal. Quantitative analysis of the state equivalent circuits, see Fig. 3, yields the normalized peak switch voltage, V_{dsmn}, as

$$V_{dsmn} = \frac{V_{dsm}}{V_i} = \frac{V_m + V_{LED}}{V_i} = 1 + \sqrt{1 + \left(\frac{\pi}{2r} T_{on\_n}\right)^2} \qquad (1)$$

Here, $r^2 = L_i/L_r$ is the inductor ratio; $V_{Ln} = V_{LED}/V_i$ is the normalized LED string voltage; $T_{on\_n} = 2T_{on}/\pi\sqrt{L_r C_s}$ is the normalized on time defined relatively to quarter of a resonant cycle of the L_r-C_s branch; T_{on} is the on time; and $V_m = v_{Cs}(t_3)$ is the peak voltage across the blocking capacitor C_s.
The normalized peak switch voltage (1) is plotted in Fig. 4 (a) as function of the normalized on time, T_{on_n}. A sample of simulation results are also shown on the plot. Excellent agreement is found.
According to (1) and confirmed by simulation, frequency variations have no effect on switch voltage. This can be considered an operational advantage of the constant T_{on} control strategy.
An approximate expression for the normalized switch rms current, $I_{ds\_rms\_n}$, was obtained and normalized with respect to the base quantity $I_b = V_i/Z_{0i}$ as

$$\mathrm{I_{ds\_rms\_n}} \cong \frac{I_{ds\_rms}}{V_i/Z_{0i}} = \left[f_n \left(\frac{r}{8}(V_{mn} - V_{Ln})^2 + \frac{V_{mn}-V_{Ln}}{r\,\pi} + \frac{\pi^2}{48}\left(\frac{T_{on\_n}}{r}\right)^3 \right) \right]^{1/2} \quad (2)$$

where $Z_{0i} = \sqrt{L_i/C_s}$ is the characteristic impedance of the L_i-C_s branch and f_n=f_s/f_{oi} is the normalized switching frequency relative to $f_{0i} = 1/2\pi\sqrt{L_i C_s}$. The plot in Fig. 4 (b) presents the comparison of the theoretically predicted versus simulated normalized switch rms current, $I_{ds\_rms\_n}$. Good agreement is found.

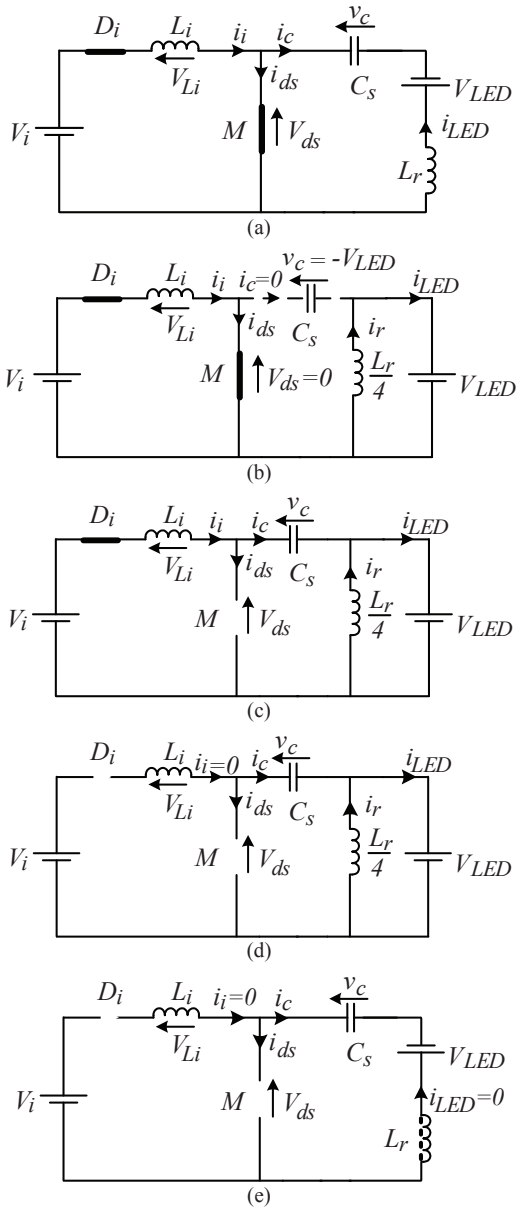

Fig. 3. Equivalent circuits of the topological states of the proposed CCD-QRLEDD: (a) State A; (b) State B; (c) State C; (d) State D; (e) State E.

The output power, P_o, of the proposed CCD-QRLEDD was obtained and normalized with respect to the base quantity $\mathrm{P_b} = \mathrm{V_{rms}^2}/\mathrm{Z_{0i}}$ as

$$P_n = \frac{P_o}{P_b} = \left(\frac{f_n}{4\pi}\right) V_{dsmn}^2 \quad (3)$$

Fig. 4 (c) illustrates the normalized power, P_n, as a function of the normalized frequency $\mathrm{f_n}$, for selected values of T_{on_n}. Within the preferred operation mode, described above, the normalized power is independent of the LED string voltage.

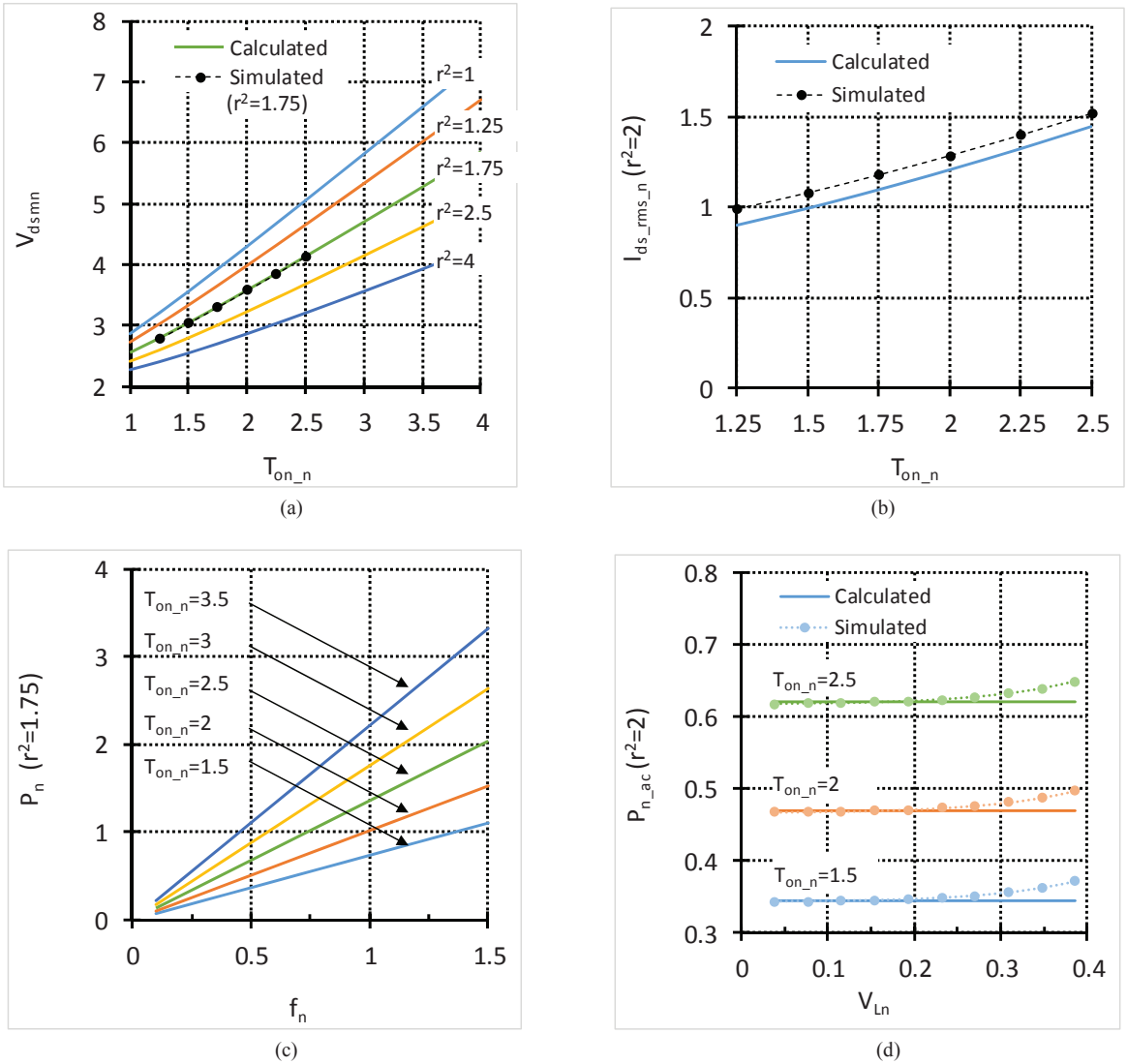

Fig. 4. Calculated vs. simulated performance indexes of the proposed CCD-QRLEDD as compared to PSIM simulation: (a) the normalized peak switch voltage, V_{dsmn}; (b) the normalized rms switch current $I_{ds\_rms\_n}$; (c) the normalized power, P_n, as function of the normalized switching frequency f_n; (d) dependence of the normalized power, P_n, on the normalized LED string voltage, V_{Ln}.

Also note the advantage of the proposed control strategy for which the normalized power is linear with the switching frequency. At low line voltage, however, an alternative resonant mode appears which causes the power to deviate from the value predicted by (3) as well as reveals some dependence on the LED string voltage. Plot in Fig. 4 (d) is generated for constant f_n=0.5, for selected values of T_{on_n} and sweeping V_{Ln} within the typical range of LED string voltage. Clearly, the error is acceptable so, for most practical purposes, (3) can be considered valid throughout the line cycle and, hence, safely used for AC power calculations.

III. Experimental Results

The proposed CCD-QRLEDD prototype was build and tested. The prototype operated from 110Vrms 60Hz line and delivered up to 25 W to LED load at 25-30 Vdc. The experimental converter had the following parameters. The diodes were: D_i- SiC Cree C3D02060F, D_o -ST STTH5L06RL; the switch-ST STP11N65M2 Rds=670mOhm Eo≈1.6 µJ @ Vds=400 V; the input inductor: L_{in}=108 µH , the coupled inductor L_r =2x27 µH (resulting in r^2=1); the series capacitor: 2Cs = 2670 pF (2200 pF || 470 pF), the bypass capacitor C_{in}=220 nF, and the output filter capacitor: C_{out} = 220 µF. No hardware optimization was attempted.

The switching frequency was varied in 40-250 kHz range. Controller on time was set to T_{on}=770 ns

resulting in t_n=1.29 using actual value of the inductors.

Experimental results are shown in Fig. 5. Input port waveforms on the line period scale appear in Fig. 5 (a). As expected, CCD-QRLEDD draws a nearly sinusoidal current from the line. The key waveforms of the CCD-QRLEDD on the switching period scale are shown in Fig. 5 (b) and strongly resemble the expected waveforms in Fig. 2 (b). The averaged line current in Fig. 5 (c) was measured at different power levels and retains good quality in a broad power range. The total harmonic distortion and the power factor of the CCD-LEDD were recorded and plotted in Fig. 5 (d). In a wide range the PF exceeds 99% and the THD is lower than 10%. Comparison of the theoretically predicted by (3) and measured power as function of switching frequency is conducted in Fig. 5 (e).

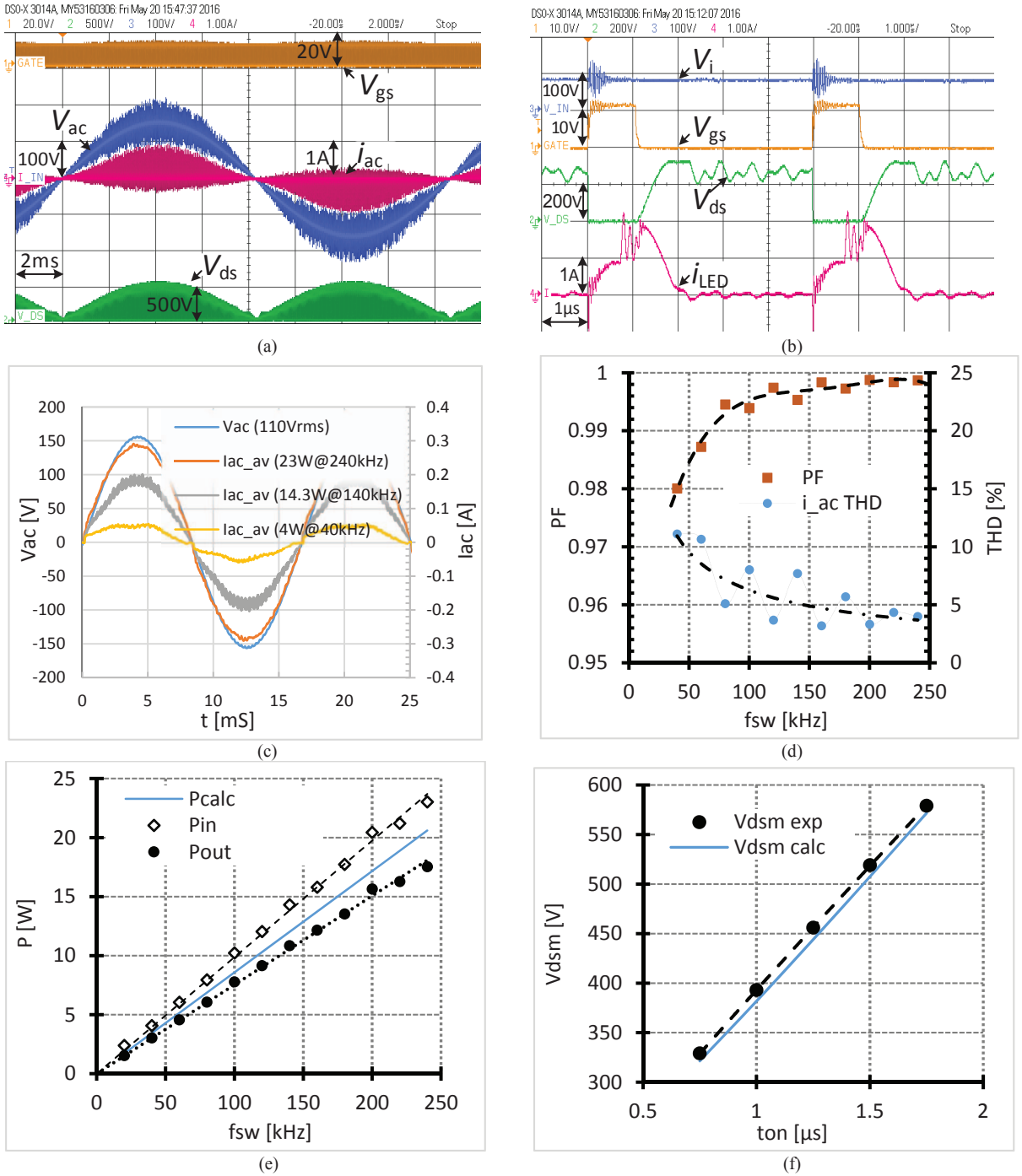

Fig. 5. Experimental results: (a) input port waveforms on the line period scale; (b) key waveforms on the switching period scale; (c) line voltage and averaged line current at different switching frequencies (power levels); (d) THD and PF performance indexes; (e) comparison of the theoretically predicted, P_{calc}, and measured power, P_{in}, P_{out}, as function of switching frequency; (f) comparison of predicted vs. measured peak switch voltage

Good agreement is found between the theoretical and experimental results. CCD-QRLEDD attained only average efficiency performance of up to 80%. It was found that converters' efficiency is strongly affected by diode conduction losses as the diode voltage drop constitutes a significant percentage of the LED string voltage. Another loss factor to consider is that the zero current switching technique, applied here, is prone to the turn-on loss. The relatively low LED string power can allow for only a minute turn on loss. The later can be improved by choosing a switch with lower parasitic capacitances and operation at reduced switch peak voltage. Comparison of the theoretically predicted by (1) and experimentally measured peak switch voltage is shown in Fig. 5 (f). Good agreement is found.

Conclusion

This paper described the principle of operation of a novel single switch quasi-resonant driver for high brightness LED lighting applications. The topology possesses important merits of simplicity, low line current distortion, capacitive isolation, and soft switching, suitable for high frequency operation. The brightness of a LED string can be controlled by either modulating the switch on time or the switching frequency. The latter is preferred. Theoretical expressions for key performance indexes were derived theoretically and verified by simulation and experiment. Good agreement was found.

References

[1] J. Y. Tsao, "Solid-state lighting: lamps, chips, and materials for tomorrow," *Circuits and Devices Magazine, IEEE*, vol.20, no.3, pp.28,37, May-June 2004.

[2] M. G. Craford, "LEDs challenge the incandescents," *Circuits and Devices Magazine, IEEE*, vol.8, no.5, pp.24,29, Sept. 1992.

[3] A. Abramovitz et al., "A Quasi-Resonant LED Driver with Capacitive Isolation," *Electronics Letters,* vol.51, no.3, pp.274-276, 25 2015.

[4] D. Shmilovitz et al., "Quasi-Resonant LED Driver With Capacitive Isolation and High PF," in *Emerging and Selected Topics in Power Electronics, IEEE Journal of* , vol.3, no.3, pp.633-641, Sept. 2015.

[5] D. Shmilovitz et al., "A Family of Bridgeless Quasi-Resonant LED Drivers" in *Power Electronics, IEEE Transactions on*, vol.31, no.3, pp.1833-1836, March 2016.

[6] A. Abramovitz et al., "Off-line capacitively-isolated quasi resonant LED driver," in *17th European Conference on Power Electronics and Applications (EPE'15 ECCE-Europe), 2015*, vol., no., pp.1-8, 8-10 Sept. 2015.

[7] Suntio, Teuvo. *Dynamic profile of switched-mode converter: modeling, analysis and control*. John Wiley & Sons, 2009.

[8] Teuvo Suntio (2012). Issues on Interfacing Problematics in PV Generator and MPP-Tracking Converters, Solar Power, Prof. Radu Rugescu (Ed.),

[9] Suntio, T.; Viinamaki, J.; Jokipii, J.; Messo, T.; Kuperman, A., "Dynamic Characterization of Power Electronic Interfaces," *Emerging and Selected Topics in Power Electronics, IEEE Journal of*, vol.2, no.4, pp.949,961, Dec. 2014

[10] S. Singer, "Gyrators Application in Power Processing Circuits,"*Industrial Electronics, IEEE Transactions on*, vol.IE-34, no.3, pp.313-318, Aug. 1987.

[11] D. Shmilovitz, I. Yaron, and S. Singer, "Transmission-line based gyrator," *IEEE Trans. Circuits Syst. Part I*, vol. 45, no. 4, pp. 428-433, Apr. 1998

[12] D. Shmilovitz, "Gyrator realization based on a capacitive switched cell," *IEEE Trans. Circuits Syst. II*, vol. 53, no. 12, pp. 1418-1422, Dec. 2006. Q3, IF=1.23, ISI=14; GS=16.

[13] A.C. Pastor et al., "Analysis and design of power gyrators in sliding mode operation," *IEE Trans. Power Appl.,* vol. 152, no. 4, pp. 821-826, Jul. 2005.